[Frontiers in Bioscience E4, 1731-1742, January 1, 2012]

Evaluation of unintended electrical stimulation from MR gradient fields

Howard I. Bassen[1], Leonardo M. Angelone[1]

[1]Division of Physics, Office of Science and Engineering Laboratories, Center for Devices and Radiological Health, U.S. Food and Drug Administration, Silver Spring, MD

TABLE OF CONTENTS

1. ABSTRACT

Exposure of patients with active implants (e.g. cardiac pacemakers and neurostimulators) to magnetic gradient fields (kHz range) during magnetic resonance imaging presents safety issues, such as unintended stimulation. Magnetically induced electric fields generate currents along the implant's lead, especially high at the distal tip. Experimental evaluation of the induced electric field was previously conducted. This study aimed to perform the same evaluation by means of computational methods, using two commercially available software packages (SemcadX and COMSOL Multiphysics). Electric field values were analyzed 1-3 mm from the distal tip. The effect of the two-electrode experimental probe was evaluated. The results were compared with previously published experimental data with reasonable agreement at locations more than 2-3 mm from the distal tip of the lead. The results were affected by the computational mesh size, with up to one order of magnitude difference for SEMCAD (resolution of 0.1 mm) compared to COMSOL (resolution of 0.5 mm). The results were also affected by the dimensions of the two-electrode probe, suggesting careful selection of the probe dimensions during experimental studies.

2. INTRODUCTION

Magnetic resonance imaging (MRI) of patients with active implants, such as cardiac pacemakers and neurological stimulators, presents safety issues that need to be carefully addressed (1). One of these safety issues is due to electric potential induced along the implants by the low-frequency - kHz range - MRI gradient fields. These potentials generate currents along the lead and an enhancement of the electric field near the distal tip of the lead (2). The issue is also present with other common devices that emit magnetic fields in the same frequency range as gradient MRI, including metal detectors and anti-theft systems. Over 100 adverse events related to unintended stimulation were reported to FDA and as a result FDA issued official alerts to cardiologists, neurologists and other clinicians (3).

Methods for evaluating the electric field induced by strong (i.e. ~ 0.1 Tesla) low-frequency magnetic fields have been studied in detail in experimental studies. Our group has recently published the measured data on the magnetically induced electric field near the distal tip of implanted leads (4). The study evaluated the electric field induced by a 1 kHz homogeneous magnetic field at the distal

tip of a lead in a saline tank, simulating a unipolar pacemaker lead in cardiac tissue (Figure 1). Computational modeling of the experimental measurement system - properly validated with measured data - is highly desirable since it allows extrapolating the results to many configurations that would otherwise be tedious or too complex to test experimentally (5, 6). The objective of this study was to implement a numerical model similar to the experimental system, compute electric field and currents induced along the lead by the low-frequency magnetic field using two commercially available software packages, and compare the results with the measured values.

A realistic numerical modeling of an active implant lead in saline or in a human body is challenging for several reasons. The geometrical characteristics of the lead, namely a length greater than 0.5 m and a diameter of the wires inside the lead less than 1 mm, require a variable grid size. The steep change of electric field – which at few millimeters from the distal tip decays to insignificant levels - requires a submillimetric resolution to model the tip and the nearby conductive medium (i.e., saline). Finally, the modeling of the thin insulation layer requires a large number of computational cells. Recent improvements in electromagnetic software and reduced cost of RAM memory allowed to overcome these limitations and to generate reasonably accurate models.

3. METHODS

3.1. SEMCAD simulations

A first set of simulations was carried out using SemcadX version 14 (SPEAG, Zurich, Switzerland) with a new Low Frequency Quasi Static Magnetic Solver. This solver uses a finite element method based on the Biot-Savart equation and an adaptive mesh gridding engine. This allowed analyzing very small objects with a submillimetric resolution for selected parts of a thin lead, while encompassing the large diameter loop in a saline tank. Computations were performed with a personal computer with 6 GB RAM and Windows 7 operating system.

3.1.1. Numerical model of saline solution with lead

The leads were modeled by an insulated wire with a 0.54 m length immersed in a saline tank. The tank had a diameter of 0.24 m and a height of 0.23 m. The electrical properties of the saline were set to $\sigma = 0.8\ S m^{-1}$ and $\varepsilon_r = 80$ (7). The wire was $6 \cdot 10^{-4}$ m in diameter, surrounded by an insulating plastic coating with an outer diameter of $4 \cdot 10^{-3}$ m. The proximal end was modeled as a non-insulated wire about $5 \cdot 10^{-3}$ m long (Figure 2). The distal tip of the lead was bluntly cut flush with the insulation, as in the COMSOL simulations. The wire was looped along the outer region of a saline filled tank. The wire was set to have electrical properties that best matched - based on the limits of the Low Frequency Quasi Static Magnetic Solver - the conductivity of copper. This was achieved with a conductivity $\sigma = 10^5\ S m^{-1}$ and relative dielectric constant $\varepsilon_r = 1$. The insulation was assigned electrical properties of Teflon (i.e., $\sigma = 0\ S m^{-1}$ and $\varepsilon_r = 2$).

3.1.2. Magnetic field source

The magnetic field source was modeled by a pair of single turn coils in the form of a modified Helmholtz coil **(8)** driven by a 1 kHz sinusoidal current of 34.7 A, simulating the output of the high-current amplifier used in the experimental measurements (4). This produced a homogeneous magnetic field in the saline with a constant magnitude of $\left\|\vec{\mathbf{B}}\right\| = 125\ \mu T$, as in the COMSOL simulations and the experimental study.

3.1.3. Electromagnetic simulations

The gridded model of the system without the electric field probe is shown in Figure 2. Areas that did not require fine detail (e.g. the saline) were meshed with a large grid (i.e., tens of mm), while the insulation around the lead and the lead wire itself were meshed with a variable sized grid with the finest resolution up to 10-4 m. This allowed to drastically reducing the number of solid rectangular voxels and cells that needed to be analyzed compared to a fixed mesh approach. Figure 2 illustrates the high resolution of the voxels generated for the insulation and wire plus the electric field probe electrodes. No breakage in the continuity of the lead wire existed, and the insulation had no gaps that could expose the wire to the surrounding saline. A range of 6 to 18 Megacells was used in the simulations to identify the most reliable data, with corresponding simulation times between 30 and 100 minutes, respectively.

3.2. COMSOL simulations

A second set of electromagnetic simulations was performed using a commercially available Finite Element Method solver (COMSOL Multiphysics 3.5, Comsol Inc., Burlington, MA, USA) and a 16-processor Xeon 2.4 GHz machine with 24 GB RAM and 64-bit Windows Server Standard operating system.

3.2.1. Numerical model of saline solution with lead

A saline solution was modeled by means of a conductive cylinder (diameter: 0.24 m, height: 0.1 m - see discussion on modeling the saline tank) (Figure 3). The electrical properties of the saline were set to $\sigma = 0.8\ S m^{-1}$ and $\varepsilon_r = 80$. The lead was modeled by means of two concentric cylinders representing the conductive wire and the insulation. The diameter of the wire was of $6 \cdot 10^{-4}$ m. Two insulation thicknesses were tested, namely $1.4 \cdot 10^{-3}$ m and $4 \cdot 10^{-3}$ m, as in the experimental study and SEMCAD simulations, respectively. The wires were revolved for 350° to form a loop with 0.19 m diameter. The proximal end was non-insulated for approximately $5 \cdot 10^{-3}$ m, similarly to both SEMCAD simulations and experimental study. The distal tip of the lead was bluntly cut flush with the insulation, as in the SEMCAD simulations. The wire was set to have electrical properties of copper (i.e., $\sigma = 6 \cdot 10^7\ S m^{-1}$ and $\varepsilon_r = 1$), whereas the insulation was assigned electrical properties of Teflon (i.e., $\sigma = 0\ S m^{-1}$ and $\varepsilon_r = 2$), as in the SEMCAD simulations.

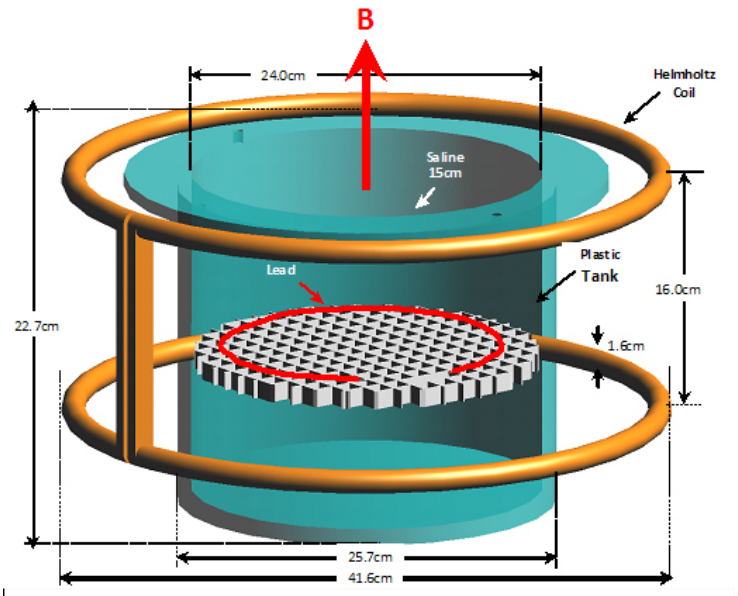

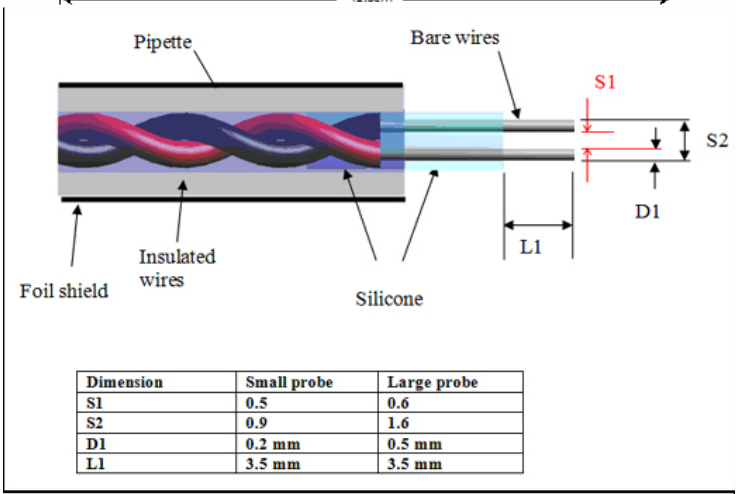

Dimension	Small probe	Large probe
S1	0.5	0.6
S2	0.9	1.6
D1	0.2 mm	0.5 mm
L1	3.5 mm	3.5 mm

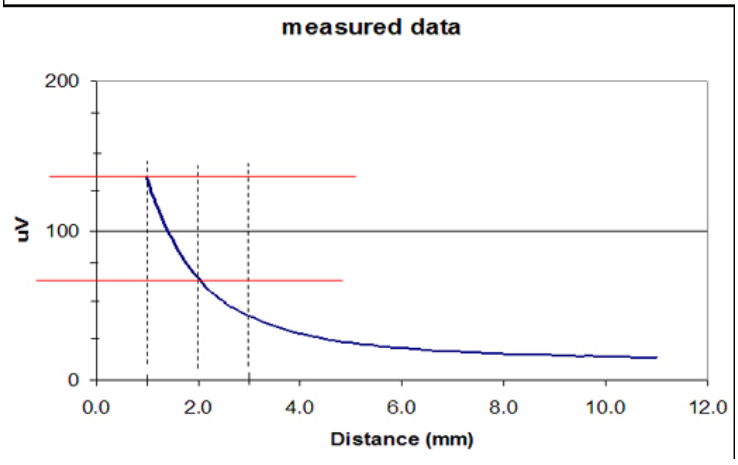

Figure 1. Experimental setup used in the experimental study (4) used for comparison of the numerical results. (Top) Modified Helmholtz coil (8) with insulated lead. (Center) Probe design and dimensions. (Bottom) Measured electric field near the distal tip. The same locations were evaluated in the computational studies (see Figure 6 and Figure 7).

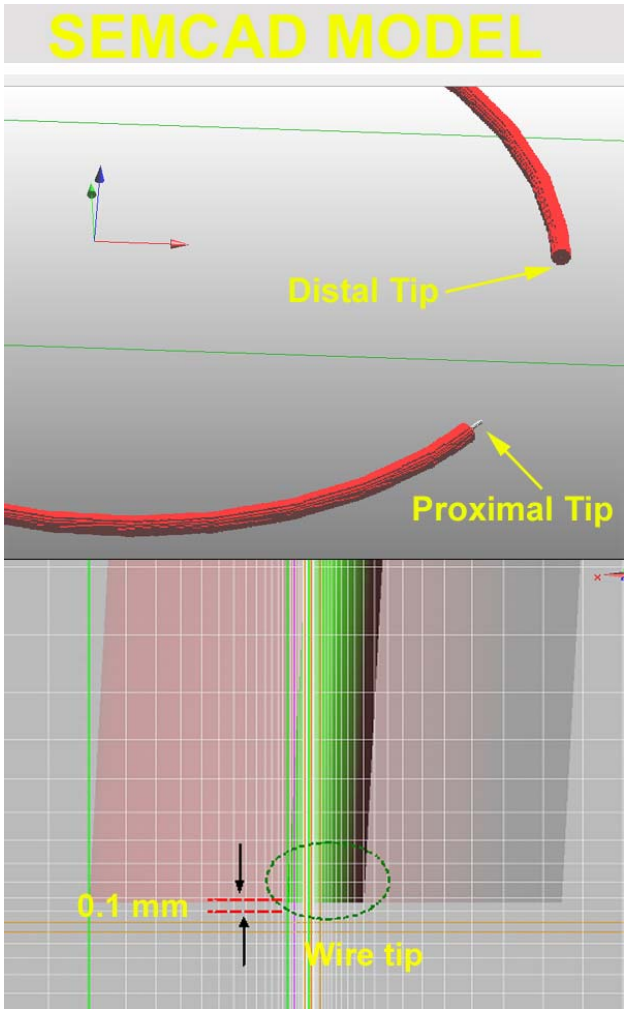

Figure 2. SEMCAD simulations with saline tank and implant. (Top) Image from SemcadX software showing simulated geometry of insulated lead. The arrow indicates the location of the proximal tip of the lead. (Bottom) Close-up view of meshed insulated wire distal tip (i.e., circled green object).

3.2.2. Magnetic field source

A homogeneous 1 kHz sinusoidal magnetic flux density perpendicular to the base of the saline cylinder was assigned as boundary condition and set to a constant value of $\left\|\vec{\mathbf{B}}\right\| = 125\ \mu T$, as in both SEMCAD simulations and experimental study.

3.2.3. Electromagnetic simulations

The quasi-static electromagnetic solver of the COMSOL Multiphysics - with electric and induced current – was selected for the simulations. The following equations were implemented:

$$\begin{cases} -\nabla\cdot\left(\left(j\omega\sigma-\omega^2\varepsilon_0\varepsilon_r\right)\vec{\mathbf{A}}+\left(\sigma+j\omega\varepsilon_0\varepsilon_r\right)\nabla V\right)=0 \\ \left(j\omega\sigma-\omega^2\varepsilon_0\varepsilon_r\right)\vec{\mathbf{A}}+\nabla\times\left(\mu_0^{-1}\nabla\times\vec{\mathbf{A}}\right)+\left(\sigma+j\omega\varepsilon_0\varepsilon_r\right)\nabla V=0 \end{cases} \quad (1)$$

where $\vec{\mathbf{A}}$ is the vector potential, $\varepsilon_0 = 8.85\cdot10^{-12}\ Fm^{-1}$ is the permittivity of vacuum, $\mu_0 = 4\pi\cdot10^{-7}\ Hm^{-1}$ is the permeability of vacuum, and $\omega = 2\pi f$ is the angular frequency with $f = 1000\ Hz$. A time-harmonic stationary solution was found using the COMSOL Multiphysics UMFPACK solver and a tetrahedral mesh. Different mesh settings were tested in order to obtain the minimum mesh size element near the distal tip available with the RAM memory limitation (Table 1). The simulation time was of up to 5 hours for a variable mesh with the finest resolution of 0.5 mm.

3.3. Comparison to analytical solution and validation of model without lead

In order to provide a simple validation of the model, the magnitude of the electric field $\left\|\vec{\mathbf{E}}\right\|_r$ induced at the outer edge of the saline without lead was computed.

Table 1. Electric fields induced near the distal tip of the simulated lead, where $\left\|\vec{\mathbf{E}}_{tip}(d)\right\|$ is the magnitude of electric field at distance d from the distal tip

SEMCAD (Insulation Outer Diameter: $4{\cdot}10^{-3}$ m)	
Distance (m)	$\left\|\vec{\mathbf{E}}_{tip}(d)\right\|$ (V m^{-1})
10^{-3}	3.875
$2{\cdot}10^{-3}$	0.980
$3{\cdot}10^{-3}$	0.465
COMSOL (Insulation Outer Diameter: $4{\cdot}10^{-3}$ m)	
Number of mesh elements	85651
Mesh size near tip	$5{\cdot}10^{-4}$ m
Distance (m)	$\left\|\vec{\mathbf{E}}_{tip}(d)\right\|$ (V m^{-1})
$2{\cdot}10^{-3}$	0.28
$3{\cdot}10^{-3}$	0.23
COMSOL (Insulation Outer Diameter: $1.4{\cdot}10^{-3}$ m)	
Number of mesh elements	74527
Mesh size near tip	$1.5{\cdot}10^{-3}$ m
Distance (m)	$\left\|\vec{\mathbf{E}}_{tip}(d)\right\|$ (V m^{-1})
$2{\cdot}10^{-3}$	0.24
$3{\cdot}10^{-3}$	0.19
Experimental data (Insulation Outer Diameter $1.4{\cdot}10^{-3}$ m)	
Distance (m)	$\left\|\vec{\mathbf{E}}_{tip}(d)\right\|$ (V m^{-1})
~$2{\cdot}10^{-3}$ *	0.1

* note experimental measurements use probe that spans 10^{-3} m

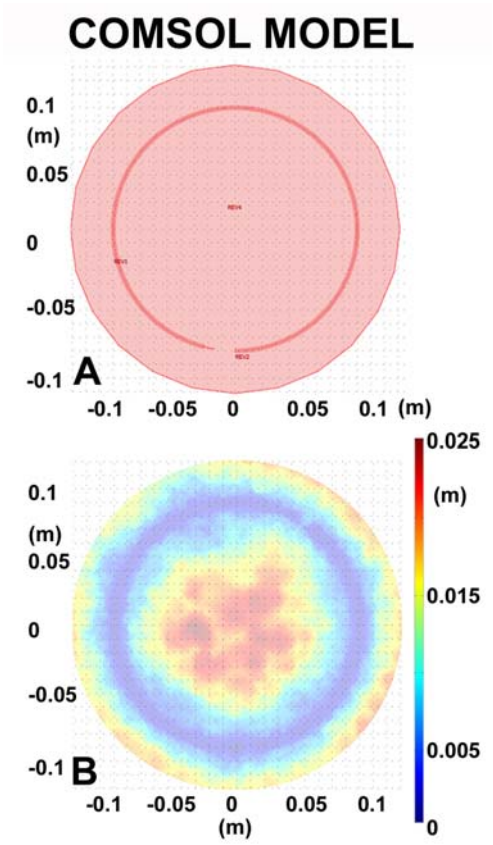

Figure 3. COMSOL simulations with saline tank and implant. (A) Axial image showing the simulated geometry of saline solution with implant. The proximal end was modeled as a non-insulated wire. (B) Mesh used for the simulations. The mesh size near the distal tip - limited by memory requirements - was approximately $5{\cdot}10^{-4}$ m. The spatial dimensions are expressed in meters.

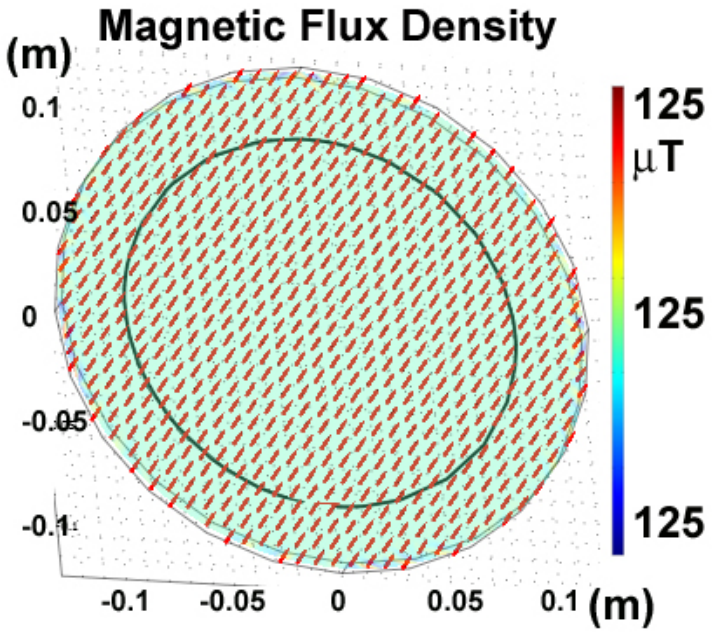

Figure 4. COMSOL simulations. The magnetic flux density at the surface of the saline tank was set to be normal and with a constant magnitude of 125 μT. The resulting magnetic flux density inside the saline (showed by the arrows) was also constant and normal to the surface.

The magnitude of electric field induced at any point in the saline solution by an incident sinusoidal magnetic field is given by the analytical equation:

$$\left\|\vec{\mathbf{E}}\right\| = \pi \cdot f \cdot r \cdot \left\|\vec{\mathbf{B}}\right\| \qquad (2)$$

where $\left\|\vec{\mathbf{E}}\right\|$ is the root mean square (RMS) magnitude of the electric field (V m^{-1}) at any point in the saline induced by a sinusoidal magnetic field, f is the frequency (Hz) of the magnetic field, r is the radial distance (m) from center of saline, $\left\|\vec{\mathbf{B}}\right\|$ is the magnitude of the incident magnetic flux density (T) from the gradient field. The derivation of this equation is shown in (9). The direction of the electric field vector $\vec{\mathbf{E}}$ is normal to a radial line drawn from the center of the tank to the outer circumference. The value of $\left\|\vec{\mathbf{E}}\right\|$ in the center of the tank is zero and increases with the radial distance from the center. The reference value $\left\|\vec{\mathbf{E}}\right\|_r$ was calculated with both SEMCAD and COMSOL at the outer edge of the saline of the model without the implant; the position chosen was the equivalent position of the distal tip of the lead in the model with the implant.

4. RESULTS

The magnitude of the magnetic flux density $\left\|\vec{\mathbf{B}}\right\|$ in the saline was uniform and equal to 124 μT in SEMCAD and 125 μT in COMSOL (Figure 4). The reference value $\left\|\vec{\mathbf{E}}\right\|_r$ without the implant was zero at the center of the saline and increased linearly toward the outer edge of the saline. There was less than 5% difference between the reference value $\left\|\vec{\mathbf{E}}\right\|_r$ calculated with both SEMCAD and COMSOL compared with the analytical solution provided by Faraday's law (see Eqn. 2 and Figure 5).

The RMS magnitude of electric field $\left\|\vec{\mathbf{E}}\right\|$ induced near the distal tip as well as the proximal tip of the simulated lead is shown in Figure 6 and Figure 7. The values of $\left\|\vec{\mathbf{E}}\right\|$ decreased exponentially along the direction tangential to the distal tip. Table 1 shows the values of $\left\|\vec{\mathbf{E}}\right\|$ along this direction, at a distance between 10^{-3} m and $3{\cdot}10^{-3}$ m from the distal tip. Values calculated with SEMCAD were 3.8 V m^{-1} at 10^{-3} m, and 0.46 V m^{-1} at $3{\cdot}10^{-3}$ m; values calculated with COMSOL were 0.3 V m^{-1} at $2{\cdot}10^{-3}$ m, and 0.2 V m^{-1} at $3{\cdot}10^{-3}$ m from the distal tip; by comparison, experimental values at $2{\cdot}10^{-3}$ m were in the range of 0.1 - 0.2 V m^{-1}.

5. DISCUSSION

5.1. Modeling the magnetic field source in SEMCAD and COMSOL

The magnetic flux density $\vec{\mathbf{B}}$ was modeled in COMSOL by setting the boundary conditions of the outer surfaces of the saline to the pre-defined magnitude of

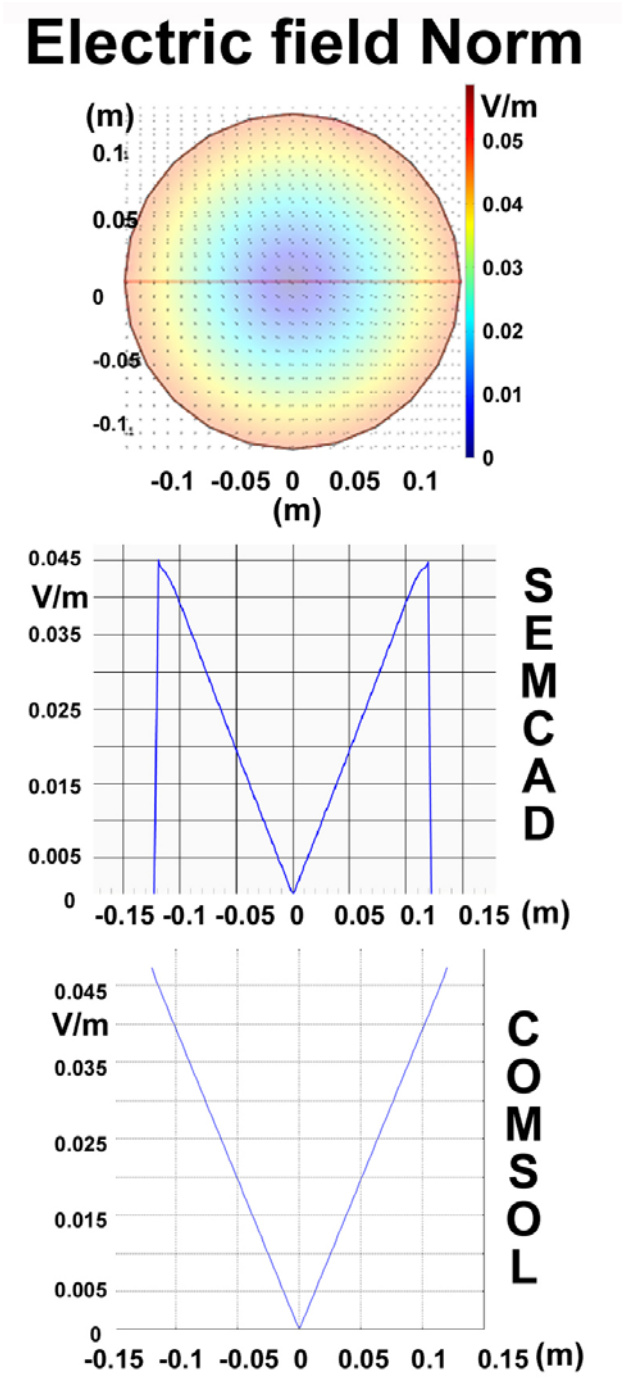

Figure 5. Calibration of SEMCAD and COMSOL simulations without implant. The electric field in saline along a path from the left to the right edge of tank through the center of the saline (Top) is shown for both SEMCAD simulations (Center) and COMSOL simulations (Bottom). The computed values of electric field matched the analytical values (see eqn. 2).

$\|\vec{\mathbf{B}}\| = 125\ \mu T$, equivalent to the value used in previous experimental measurements, and with the magnetic flux density vector oriented normally with respect to the surface of the tank. Figure 5 illustrates the resulting electric field in saline from edge to edge passing through the center of the saline cylinder. The height of the saline tank model in COMSOL was limited to 0.1 m to reduce the memory computational requirements. The value of magnetic flux density incident in the lead was not influenced by this limitation and was uniform, as in both SEMCAD simulations and experimental measurements (Figure 5).

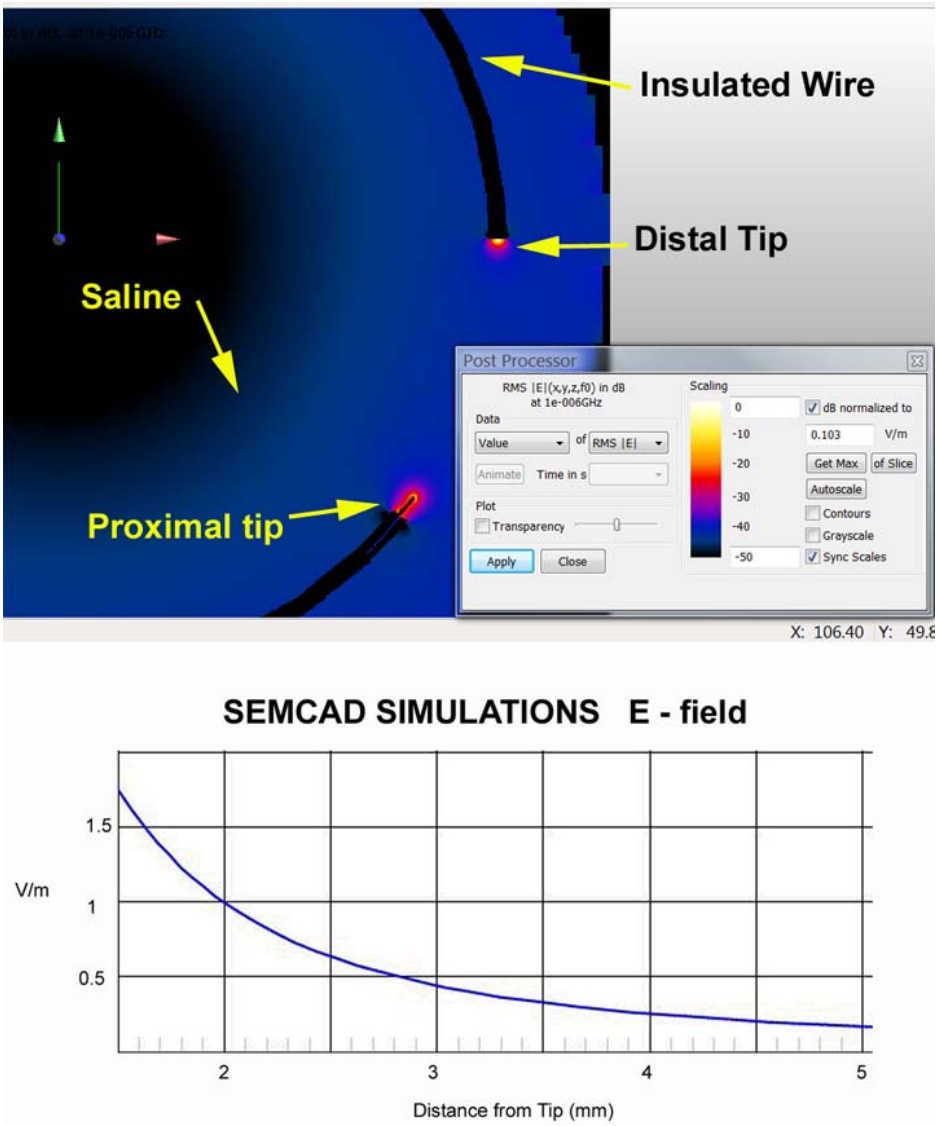

Figure 6. SEMCAD simulations with implant. (Top) Spatial map of electric field RMS magnitude $\left\|\vec{\mathbf{E}}\right\|$ in the saline near both the proximal and the distal tip. (Bottom) Linear plot of $\left\|\vec{\mathbf{E}}\right\|$ in the saline near the distal tip, along a direction tangential to the wire.

Conversely, the SemcadX solver did not allow imposing the incident magnetic flux density $\vec{\mathbf{B}}$ directly. A uniform magnetic field was generated by means of a current loop generator at 1 kHz flowing in a pair of single-turn current loops. To calibrate the model, one initial simulation was run with a 1A current generator, which resulted in a uniform magnetic flux density with RMS magnitude of $\left\|\vec{\mathbf{B}}\right\| = 3.6\ \mu T$. The final desired value of $\left\|\vec{\mathbf{B}}\right\| = 124\ \mu T$ was obtained by linearly scaling the current in the generator to 34.7 A. Although MRI gradient fields are oriented along all of the three Cartesians directions, this study evaluated a magnetic field normal to the implant lead, representing a worst case scenario.

5.2. Modeling the distal tip, proximal tip, and stimulator pulse generator

The distal tip of the lead in both SEMCAD and COMSOL models was bluntly cut flush with the insulation. This modeled a worst case scenario, since the previous experimental study (4) showed that a distal tip bluntly cut flush with the insulation produced a higher electric field in the adjacent saline when compared to a distal tip protruding past the insulation. The metallic case of the stimulator pulse generator was not included in the computational model and the proximal end of the wire had insulation removed for $5{\cdot}10^{-3}$ m, serving as the reference (return or ground) electrode (Figure 2 and Figure 3). The previous experimental study showed that this resulted in the same

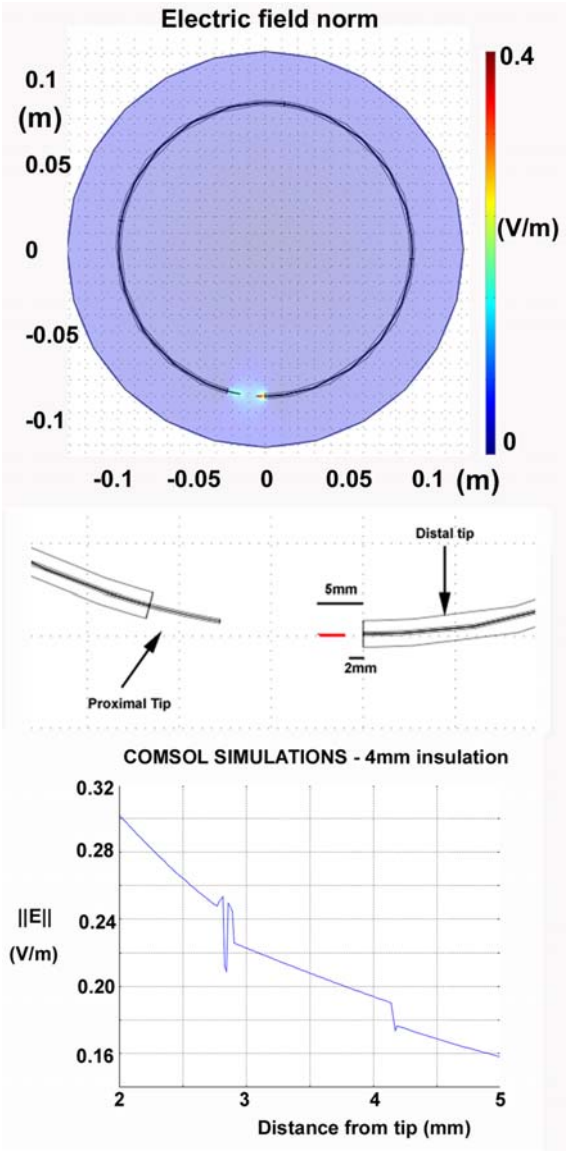

Figure 7. COMSOL simulations with implant. (Top) Axial view of the electric field magnitude in the saline tank. The area near distal tip used for the electric field plot is indicated by an arrow and shown in a zoomed view on the center of the figure. The red line, between $2 \cdot 10^{-3}$ m and $5 \cdot 10^{-3}$ m from the tip, indicates the path used to plot $\left\|\vec{\mathbf{E}}\right\|$ in the bottom graph. (Bottom) $\left\|\vec{\mathbf{E}}\right\|$ near the distal tip (i.e. red line), along the direction tangential to the wire; as in both SEMCAD simulations and experimental measurements, the electric field decreased exponentially.

electric field strength adjacent to the distal tip compared to a connection to the case of an actively pulsing pacemaker stimulator (4).

5.3. Modeling the lead insulation

The diameter of the wire was $6 \cdot 10^{-4}$ in both SEMCAD and COMSOL, modeling the same lead diameter used in the experimental study. The insulation of the lead modeled in SEMCAD was $4 \cdot 10^{-3}$ m, to avoid that – with a fixed spatial resolution of the modeled grid – parts of the lead were not directly in contact with the saline tank. To test the effect of the insulation, both $1.4 \cdot 10^{-3}$ m and $4 \cdot 10^{-3}$ m insulation models were tested in COMSOL, as in the experimental study and in SEMCAD, respectively. The COMSOL results showed a 20% - 30% effect of these values of insulation on the overall electric field at a $2 \cdot 10^{-3}$ m distance from the distal tip (Table 1).

5.4. Effect of mesh size and reduced resolution on COMSOL simulations

Because of RAM memory requirements, the minimum mesh size produced by COMSOL was

Table 2. Effect of the probe design and dimensions in the SEMCAD simulations and comparison with experimental data

Electric field: Simulations vs. Experimental data			
		probe dimensions (L: Length, D: Diameter)	E_{sim}/E_{exp}
Simulations	Probe #1	$4 \cdot 10^{-3}$ m (L) x $2 \cdot 10^{-4}$ m (D)	1.8
	Probe #2	10^{-2} m (L) x $2 \cdot 10^{-4}$ m (D)	1.2
	Probe #3	$2 \cdot 10^{-2}$ m (L) x $2 \cdot 10^{-4}$ m (D)	0.6
Experimental data		$3.5 \cdot 10^{-3}$ m (L) x $2 \cdot 10^{-4}$ m (D)	1

approximately $5 \cdot 10^{-3}$ m near the distal tip. This was in contrast to the submillimetric resolution used in SEMCAD with less physical computer (RAM) memory. As a consequence of this limitation, the closest distance from the distal tip where the electric field could be accurately analyzed with COMSOL was 1 mm.

5.5. Computation of electric field at the tip of the simulated lead and comparison with experimental results

The maximum resulting induced electric field $\|\vec{\mathbf{E}}\|$ was localized near the distal tip of the simulated lead. In all cases (i.e., SEMCAD, COMSOL, and experimental study) the electric field decreased exponentially along the direction parallel to the distal tip (Figures 1, 6, and 7). The highest mesh used in the SEMCAD simulations (i.e., 10^{-4} m resolution near the distal tip compared to approximately $5 \cdot 10^{-4}$ m in the COMSOL simulations) allowed obtaining highest values of electric field near the distal tip and an increased gradient of electric field. The mesh size of the COMSOL simulations resulted in an averaged value of electric field of approximately 0.2 V m^{-1} at 3 mm. Notably, the values were within the same range (~ 0.1 – 0.2 V m^{-1}) of the experimental study.

5.6. Computational uncertainty

There are several sources of uncertainties/errors that occur when measuring highly localized electric fields with a probe of finite dimensions, including spatial averaging, field perturbation, probe positioning, and electromagnetic pickup. The previous experimental study (4) pointed out measurement uncertainties of electric fields when the region of interest was extremely close to the tip of a simulated or actual stimulator lead.

5.6.1. Spatial averaging

One source of uncertainty is related to the changes of electric fields in space. The electric field magnetically induced at the tip of a lead has large spatial gradients, with significant changes in magnitude over a single millimeter. Spatial averaging of the electric field occurs over the region occupied by the probe tips ($9 \cdot 10^{-4}$ m wide x $3.5 \cdot 10^{-3}$ m deep in (4).) This averaging produces a reduction in the measured value of the electric field compared to the true field point value. The uncertainty is greatest when the distance between the probe and the lead is the same or less than the probe tip size.

5.6.2. Field perturbation

Another type of measurement uncertainty is due to perturbation of the electric field by metallic probe electrodes. This uncertainty is greatest when the distance between the probe and the lead is the same or less than the probe tip size. This perturbation makes the measured value of the electric field lower than the true value. This uncertainty diminishes with increasing separation between the probe and the tip of the lead.

5.6.3. Uncertainties due to probe positioning

A third measurement uncertainty is due to the error and repeatability associated with determining the true position of the probe tip with respect to an implant lead. For the mechanical system used in (4), the positioning error and repeatability was about 10^{-4} m. The measurement uncertainty due to this factor diminished as the separation between the probe and the implant lead increased. As shown in Figure 6, a change of 10^{-4} m in position generates a change of the computed electric field value of about 20%.

5.7. Effect of the presence of a physical measuring probe

As shown in (4), the probe used to measure the electric field introduces certain measurement uncertainties. In order to understand the effects of field perturbation by the probe, a computational model that included a two-electrode probe was generated with SEMCAD. The probe closest electrode was placed at various distances from the distal tip of the simulated implant lead wire. The probe was modeled in SEMCAD as two short, parallel wires (or electrodes) each having a diameter of $2 \cdot 10^{-4}$ m and spaced $5 \cdot 10^{-4}$ m apart. The electrical properties of the electrodes were chosen to model a perfect electrical conductor. The best matches - based on the limits of the Low Frequency Quasi Static Magnetic Solver in SemcadX - were conductivity $\sigma = 10^5 \ S\,m^{-1}$ and relative dielectric constant $\varepsilon_r = 1$. A voltage sensor was included across the two electrodes (as shown in Figure 8). The voxel models for several configurations of the simulated lead and electric field probe are shown in Figure 8. Many variations of the parameters of probe size (i.e., diameter, length separation from the wire distal tip position) were evaluated. The numerical results were compared with data measured with an electric field probe in (4) (see Table 2). When the electric field measurement probes were included in the model and their effects on the local electric field were therefore accounted for, the computational results agreed well (±10%) with the experimental ones. One revealing part of the study was achieved by observing the changes of voltage across the probe when the length of the probe wires was varied. The length of the electrode wires was varied from $4 \cdot 10^{-3}$ m to $20 \cdot 10^{-3}$ m. The simulated values were significantly lower with long (i.e., $20 \cdot 10^{-3}$ m) electrode wires. This was attributed to spatial averaging of the field, highly non uniform and very low above and below the exact location of the distal tip. Also, the large metallic electrodes likely perturbed the field when they were very close to the source of the fields (i.e., at the distal tip). This effect could explain the differences between the computed

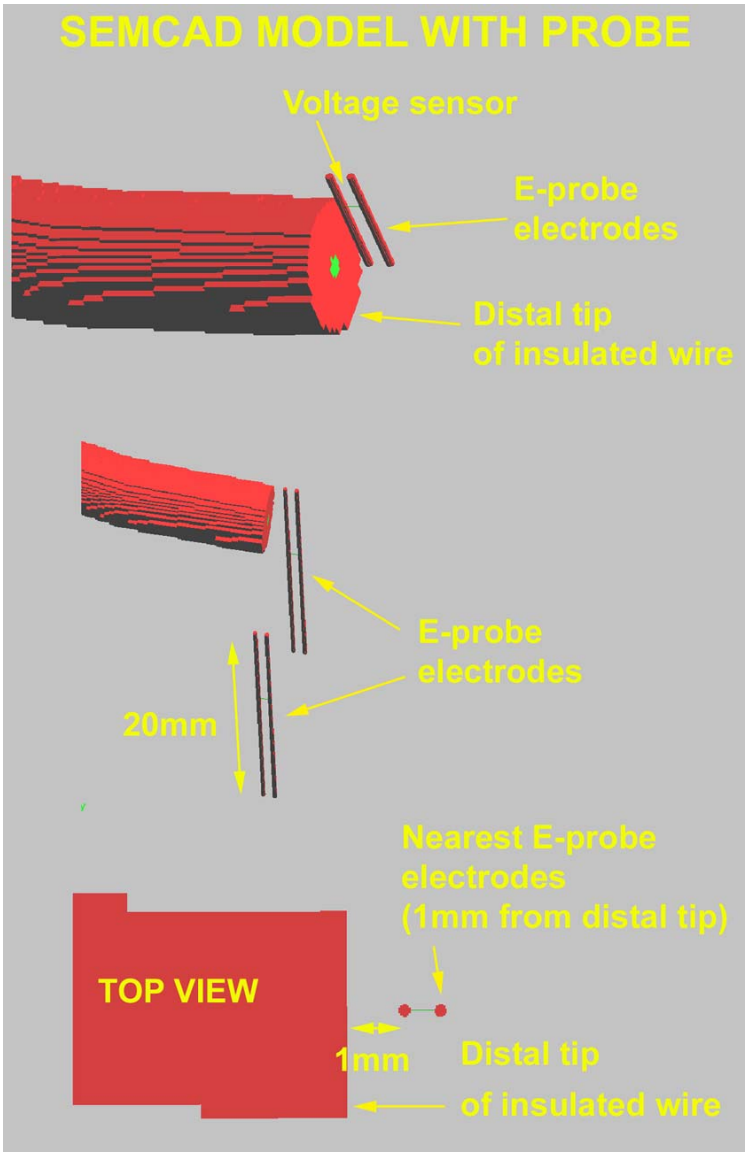

Figure 8. Probe design and dimensions used in SEMCAD simulations to evaluate the effect of the probe.

values of electric field versus the experimentally determined electric field as derived from measured voltages in our probe.

6. CONCLUSIONS

There is a significant need to evaluate the safety of implanted medical devices utilizing long, thin, insulated stimulation leads or conductive wires exposed to kHz-range magnetic fields, to avoid unintended cardiac or neural stimulation. This is often accomplished by evaluating the electric field with invasive connections of wires made inside the implanted device or its lead connectors. However, these invasive modifications can only be made by the device manufacturers. Even when invasive wires are attached, they modify the magnetic field coupling to the device under test, adding measurement uncertainties for unintended stimulation.

This study of the electric field distribution induced by low-frequency sinusoidal magnetic fields used non-invasive computational methods, and compared the results to prior experimental measurements with a two-electrode probe. The electric field was computed at locations of few mm from the distal tip of a lead immersed in a saline tank. Two commercially available electromagnetic solvers were used, namely SemcadX and COMSOL Multiphysics, both based on the finite element method.

Reasonable agreement in the electric field values obtained by the two computational models existed at a distance of two or more mm from the lead, with

uncertainties due spatial averaging related to the numerical grid used in the simulations. The submillimetric resolution used in SEMCAD with less physical computer (RAM) memory allowed calculating the electric field at distances of up to 1 mm from the distal tip. In the experimental study, the probe outer dimensions were $9 \cdot 10^{-4}$ m; therefore the experimental data measured at distances closer than 1 mm was not accurate. The computational models agreed well (±10%) with the experimental results when the electric field measurement probes were included in the model and their effects on the local electric field were therefore accounted for. Measurements with smaller probes may provide an accurate value of magnetically induced electric fields at distances closer than 1 mm from the distal tip.

7. ACKNOWLEDGMENTS

The mention of commercial products, their sources, or their use in connection with material reported herein is not to be construed as either an actual or implied endorsement of such products by the Department of Health and Human Services. The authors would like to thank Seth Seidman for the useful comments and insights and Isaac Chang for the support with the COMSOL simulations.

8. REFERENCES

1. E. T. Martin, J. A. Coman, F. G. Shellock, C. C. Pulling, R. Fair, and K. Jenkins, Magnetic resonance imaging and cardiac pacemaker safety at 1.5-Tesla. *J Amer Coll Cardiol*, 43, 1315–1324 (2004)

2. A.W. Guy, Calculation of Field Enhancement due to external leads and implants in contact with Tissues. In Appendix G, NCRP Report 67: Radiofrequency Electromagnetic Fields: Properties, Quantities and Units, Biophysical Interaction, and Measurements, 108-111 (1981)

3. D. B. Burlington. Important Information on Anti-Theft and Metal Detector Systems and Pacemakers, ICDs, and Spinal Cord Stimulators. Center for Devices and Radiological Health, Food and Drug Administration, September 28, 1998

4. HI Bassen and GG Mendoza, In-vitro mapping of E-fields induced near pacemaker leads by simulated MR gradient fields. BioMedical Engineering OnLine 8:39 (2009)

5. M. Bencsik, R. Bowtell, and R. Bowley. Electric fields induced in the human body by time-varying magnetic field gradients in MRI: numerical calculations and correlation analysis. *Phys Med Biol* 52, 2337–2353 (2007)

6. CM Collins, Numerical field calculations considering the human subject for engineering and safety assurance in MRI. *NMR Biomed* 22(9):919-26 (2009)

7. A. Stogryn, Equations for calculating the dielectric constant of saline water. IEEE Trans on MicrowaveTheory and Techniques, August, pg 733-736 (1971)

8. V. Buzduga, DM Witters, JP Casamento, W Kainz, Testing the immunity of active implantable medical devices to CW magnetic fields up to 1 MHz by an immersion method. IEEE Trans Biomed Eng 54 (9), pp. 1679-1686, (2007)

9. HI Bassen, T Litovitz, M Penafiel, R Meister, ELF In Vitro Exposure Systems for Inducing Uniform electric and Magnetic Fields in Cell Culture Media. Bioelectromagnetics 13, 183-198 (1992)

Key Words: Pacemaker, Neurostimulator, Electric Field Enhancement, Spatial Resolution, Probe, kHz, Electromagnetism

Send correspondence to: Howard I. Bassen, 10903 New Hampshire Avenue, WO62 Rm. 1112, Silver Spring, MD 20993-0002. Tel: 301-796-2595, Fax: 301-796-9927, E-mail: howard.bassen@fda.hhs.gov

http://www.bioscience.org/current/vol4E.htm